ISSN: 2723-9535

Available online at www.HighTechJournal.org

HighTech and Innovation Journal

Vol. 6, No. 4, December, 2025

Noise Separation Techniques for Accurate Substation Anomaly Detection: An Intelligent Methodology

Xiaomeng Zhai [1], Jingyi Wang [1], Xi Cheng [1*], Licai Yan [2], Dianmao Zhang [2]

[1] *State Grid Jiangsu Electric Power Co., Ltd. Economic and Technical Research Institute, Nanjing 210008, Jiangsu, China.*

[2] *Unis Software System Co., Ltd., Beijing 100084, China.*

Received 10 December 2024; Revised 11 September 2025; Accepted 02 October 2025; Published 01 December 2025

Abstract

To better monitor and characterize sounds produced by substations, this study aims to separate sounds produced by the equipment from environmental ambient noise as a means of improving the relevancy (and ultimately reliability) of the power grid. To do so, we propose a deep learning-based noise monitoring system in an end-network-cloud architecture that enables remote data collection, analysis, and management. This is achieved by developing a deep learning-based noise monitoring system, enabling remote data collection, processing, and management. The proposed method consists of two basic components: a self-designed Panel Response Acquisition device that can collect sufficient acoustic information, and a refined Deep Belief Network (DBN) that is trained with a Dynamic version of the Dwarf Mongoose Optimizer (DDMO) to improve the accuracy of the noise separation process. The performance of the DBN/DDMO model is 13.1 dB for SI-SDRi and 15.7 dB for SDRi, which are large improvements for SI-SNRi and SDRi over AlexNet and CNN-VGG19. This approach minimizes SPL deviations, as shown by a thorough computation regarding several data sets; therefore, it guarantees precise noise quantification under disturbing sounds. By allowing for proactive identification of unusual noise levels, this research supports predictive maintenance methods that can avoid sudden failures and improve the overall reliability of substations.

Keywords: Substation Noise Monitoring; Deep Learning; Deep Belief Network; Dynamic Dwarf Mongoose Optimization Algorithm; Noise Separation; Anomaly Detection; Acoustic Analysis.

1. Introduction

The power distribution in electrical grids depends highly on how efficiently the substations will function smoothly and reliably [1]. These substation components are important to transform and distribute electricity for the fulfillment of various consumer needs [2]. However, abnormal noise levels can give an indication of partial malfunctioning or failure in the substation equipment and may lead to serious, disruptive, and costly impacts [3]. Therefore, effective noise monitoring and analysis are required for reliable operation of the substation and to maintain power grid stability [4].

Traditional noise monitoring methods are usually performed by manual inspection and simple noise measurement, which are time-consuming, labor-intensive, and prone to human error [5]. Furthermore, it is very difficult to identify the difference between normal and abnormal noise, especially in cases with environmental background noise [6]. In this regard, there is an increasing demand for a novel solution that will be able to monitor substation noise accurately and effectively, separate the noise generated from the equipment itself from the background noise, and detect anomalies.

* Corresponding author: xicheng13031@outlook.com

http://dx.doi.org/10.28991/HIJ-2025-06-04-020

Recent developments in deep learning and acoustic analysis have significantly increased the possibilities of noise monitoring systems [7]. Deep learning frameworks have shown their efficiency in various audio-related applications, such as noise separation and anomaly detection [8]. Using large datasets and state-of-the-art computational methods, these models can detect complex patterns and features in acoustic data to enable more accurate and automated noise analysis [9].

Zhou et al. [10] explored NLOS (non-line-of-sight) or LOS (Line-of-sight) identification in substation fields based on both feature fusion approaches and deep learning networks. Environments of high-voltage substations were used for collecting the data on measurements of channels, covering both the cases of LOS and NLOS. Manually extracted and original channel features were extracted for the creation of datasets. In the model, the hybrid fusion approach was utilized to find the correlation among channel features and avoid data inundation due to dimensional differences of input features. In performance assessment, the recognition accuracy achieved by the model was 98.95%, and it had good strength in noise and manageable calculation complexity.

Fan et al. [11] evaluated the proportion of noise annoyance that was made via substations to the people in that vicinity. A noise forecasting network was made on the basis of the CNN and Transfer Learning (TL). The input of the study was the noise spectrum, while the output of target was the subjective assessment outcome. The AlexNet was utilized with corresponding variables and an adapted output layer serving like the pre-training network. The findings demonstrated that all data sets exhibited convergence once 90 iterations were accomplished when the mini-batch scope was 4, 8, 16, and 32. The RMSE (Root Mean Square Error) for each validation set was below 0.355, and the loss for all validation sets was under 0.067. As the size of the mini-batch was raised, the loss, RMSE, and MAE (Mean Absolute Error) of the validation set rose steadily, whereas the training duration and the quantity of iterations were reduced continuously. The eventual CNN model exhibited high robustness and accuracy, and the disparity between the subjective evaluation and the predictive outcome was between 7% and 2%.

Shao et al. [12] offered a diagnosis method on the basis of MTF (Markov transition field) and CNN (Convolutional Neural Network) for substation boundary intrusion identification. The one-dimensional signals were transformed into 2D images employing MTF in order to better represent the characteristics of intrusion-like signals, providing more detailed signal information compared to traditional feature extraction methods. The CNN-VGG19 model was used for its strong ability to identify features of images. The findings of the current study revealed that the mean identification rate of the 6 intrusion occasions was 96.7%, and the mean identification rate of the noise occasions was 99%.

Yang & Li [13] adjusted distributed calculating via making an actual-time distributed calculation framework, employing accessible technology with the purpose of storing the online reviewing of sound data in calculating framework for processing the data with the purpose of obtaining the aim of automated fault analysis and diagnosis.

The findings indicated that distributed calculating could enable visualizing equipment data, storage, and intelligent analysis within the substation, offering support of data for fault detection. Additionally, the process of training yielded fitting accuracy rates and training procedures of 99.353% and 95.123% for the ANN model, with a fitting accuracy proportion of 95.478%. Furthermore, the error between the actual value and the predicted value of the five signals of sound in the fault detection procedure was 5%. As a result, the ANN model could precisely recognize all fault sounds of the substation and fulfilled the aim of fault detection.

Chen et al. [4] presented a substation noise monitoring model that was modeled on the basis of an end-network-cloud framework that aimed to learn and investigate the noise of a substation. Besides, an unusual noise level was reported, which could exceed national standards regarding substation maintenance and operation. A noise separation smart algorithm was recommended using a Conv-TasNet (Convolutional Time-Domain Audio Separation Network), a DPRNN (Dual-Path Recurrent Neural Network), or a DPTNet (Dual-Path Transformer Network). The noise separation optimizers based on deep learning were found to work better when compared to the classic spectral subtraction approaches. In the case of SDRi and SI-SNRi, Conv-TasNet, DPRNN, DPTNet, and traditional spectral subtraction had the results of 12.6 and 11.8, 13.6 and 12.4, 14.2 and 12.9, and 4.6 and 4.1, respectively. From the experiment results, DPRNN and DPTNet are found to work very effectively in the separation of noise generated from substation equipment and environmental noise. Moreover, 91% of the separated data maintained differences in the level of sound pressure less than 1 dB, showing the efficiency and effectiveness of the suggested optimizer in the separation of interference noise and accurately preserving the degree of sound pressure of substation noise.

In this paper, an advanced noise monitoring system has been proposed for substations, which is based on a deep learning framework to overcome the limitations of traditional methods. The system architecture follows the end-network-cloud architecture and supports remote and centralized noise data collection, analysis, and management. At the core of our system lies a self-designed noise acquisition device that captures acoustic characteristics with high accuracy, hence providing full information about substation noise levels and sources.

Although progress has been made, available literature review was not consistently effective in distinguishing substation equipment signatures from environmental background noise. In order to overcome the shortcomings of traditional methods, this paper has designed an advanced noise monitoring system for substations based on deep learning framework. The end-network-cloud model brings the system abstraction, which supports the remote centralized noise data collection, noise analysis, and management. The noise acquisition device (custom-designed with an array of microphones and acoustic sensors) serves as the cornerstone of the system, enabling to capture acoustic features with unparalleled precision and gain a holistic view of substation noise continuity and source identification.

Here, an advanced version of a donor-based noise separation algorithm (DBNS) is presented that can separate sound from substation equipment from atmospheric noise (environmental background noise) more reliably. Using the dynamic version of the Dwarf Mongoose Optimization Algorithm, the DBN model is further enhanced to improve its noise-separation capability. The use of deep learning methods promises to achieve better robustness and accuracy compared with traditional methods in terms of noise separation.

Moreover, the effectiveness of the system has been evaluated under different practical conditions to establish its reliability. Post-separation data confirms system noise or sound pressure level deviations and still allows for accurate substation noise analysis in the presence of interfering noises. This study enables a stable body of knowledge in the thriving area of intelligent noise monitoring and anomaly detection of quintessential infrastructures as deep-learning techniques facilitate a holistic transformation towards cutting-edge operation and maintenance processes of substations.

The rest of this paper is structured as follows. Section 2 presents Deep Belief Networks (DBNs), as well as their implementation in order to separate noises. In Section 3, the new Dynamic Dwarf Mongoose Optimization (DDMO) algorithm is presented by explaining its motivation, the population initialization, and its operational model. In Section 4, the methodology is detailed; specific attention is given to the problem statement, device design for noise collection, techniques of noise separation, and the implementation of sound level algorithms. In Section 5, simulation results (time weighting, frequency weighting, measure indicators, and comparative analysis) are explained. Finally, Section 6 ends with a summary of insights and implications for future work.

2. Deep Belief Network

DBNs, or Deep Belief Networks, represent deep unsupervised learning techniques in artificial intelligence. It uses generative algorithms and possibility distributions. It is an evolution of the Boltzmann machine and has been developed by Geoffrey Hinton. The basic principle of Deep Belief Networks is to abstract features using multiple layers of "hidden units". These networks find a very broad application in tasks like pattern recognition, especially in natural language processing, computer vision, and speech recognition [14].

Significantly, one of the advantages is that DBNs can relieve their dependence on structured data by extracting information from the unstructured data [15]. These are especially important in circumstances where structured data are low; for example, text processing and image classification [16]. By design, the DBN has also proven to perform well in different datasets as well as in different task types. This is constituted by multiple layers of interlinked neurons; each was designed to present inputted data in a particular order.

The input layer is the first layer in the network. Features of the input data are extracted by the hidden neurons in the hierarchical layers. The output layer, the last layer of the network, is used for the organization or prediction of data input. After training procedures, all the layers can be used to identify patterns in the input data and make predictions.

Thus, the identification of a configuration of the Deep Belief Network algorithm that best increases the likelihood of any given data becomes of utmost importance [17]. The best option or a good optimal subsequent estimation method is required. DBN can be achieved with the aid of several other techniques like backpropagation and bio-inspired strategies. Besides that, regularization techniques such as weight decay and dropout would avoid overfitting, making the model more generalized.

The structure of the DBN can be enhanced by utilizing an improved model of the DBN strategy. The quantity of input nodes has been determined by the features of data, while the quantity of output nodes is specified by the classifications. Therefore, this approach is crucial for achieving optimal results. Understanding the structure of the base layer is essential, considering the number of neurons in hidden layer for all the layers and the scope of particles. Consequently, a potential initial set of systems will be available according to a dynamic version of dwarf mongoose optimization algorithm.

To address the challenge of effectively optimizing the boosted individuals, it is crucial to identify the individuals. This will ensure that the appropriate equation is documented. Figure 1 illustrates a typical Deep Belief Network.

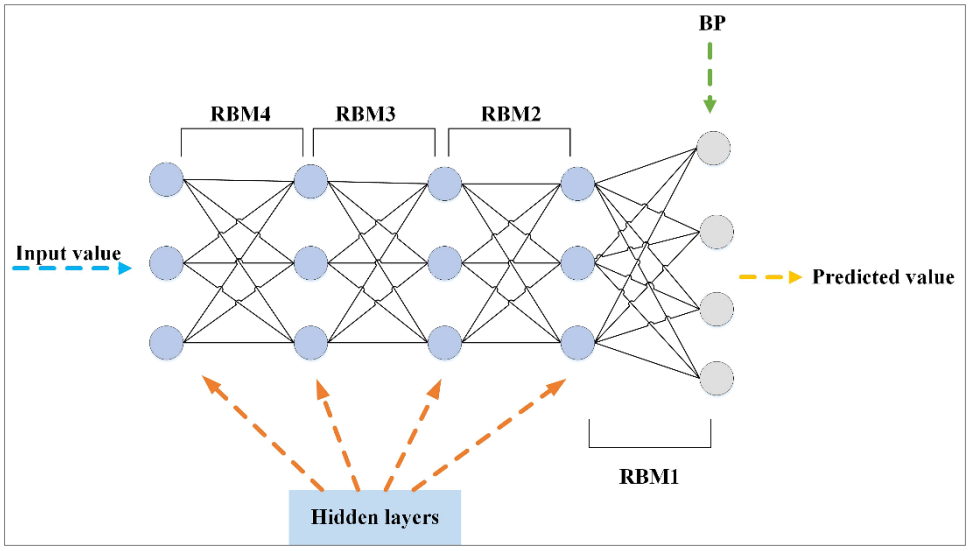

Figure 1. The block diagram of DBN

The combination of the Deep Belief Network and Dynamic Dwarf Mongoose Optimization algorithm (DBN/DDMO) is set to be trained utilizing the training set. The DBN/DDMO model has been employed to select the most appropriate fitness individuals, and these individuals will be used to construct the network structure for effectively separating electrical equipment noise from environmental noise.

The initial stage involves identifying several sets of RBMs through the opportunistic divergent comparison approach to initiate the preliminary process. Once the pre-training stage has been accomplished, the RBMs are broken down to construct the DBN, which is then adjusted employing error variants back-propagation. Ultimately, the algorithm relies on the DBN architecture that has been advanced and implemented employing the suggested technique, as illustrated in Figure 2 depicting the process of improving a classification method for intrusion recognition.

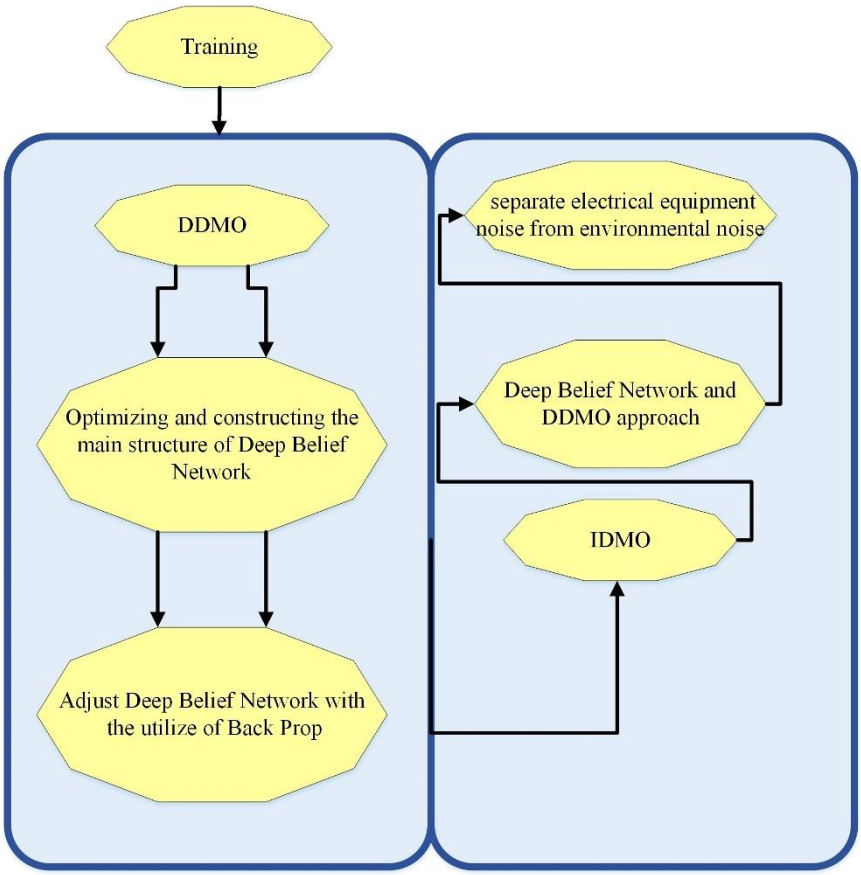

Figure 2. The phases of enhancing and progressing an identification of intrusion categorization method

The fitness function has been described in Equation 1 and is used to optimize the efficacy standard of the DDMO algorithm in the Deep Belief Network.

$$F = (1 - \beta_1 + \beta_2 + \beta_3 + \beta_4 + \beta_5) \times N_E + \beta_1 \times \frac{n}{\mathrm{Z}^{\max}} + \beta_2 \times \frac{\sum_i x_i}{\mathrm{m} \times \mathrm{S}^{\max}} + \beta_3 \times FPA + \beta_4 \times FNA + \beta_5 \times RA \quad (1)$$

where, the quantity of errors has been demonstrated by N_E, the value of middle layer has been represented by m, the entire quantity of middle layers has been indicated by $\sum_i x_i$, and the highest quantity of layers in the DBN has been shown by $\mathrm{Z}^{\max}$. The weight coefficients have been illustrated by $\beta_1 + \beta_2 + \beta_3 + \beta_4 + \beta_5$, ranging between [0, 1]. Then, the False Negative Amount (FNA), False Positive Amount (FPA), and Recognition Amount (RA) have been calculated in the following manner:

$$RA = \frac{FN}{FN + TP} \quad (2)$$

$$FNA = \frac{FN}{FN + TN} \quad (3)$$

$$FPA = \frac{FP}{TP + FP} \quad (4)$$

Evaluating intrusions involves various procedures to classify methods, such as identifying false positives, recognizing accuracy, precision (ACC), and assessing false negatives. These evaluations can be utilized to improve network configuration. In other words, as optimization increases, fitness decreases. The fitness is defined below:

$$ER = 1 - ACC \quad (5)$$

where, the precision of categorization has been demonstrated by ACC, which is calculated subsequently:

$$ACC = \frac{TP + TN}{TP + TN + FP + FN} \quad (6)$$

While recognizing the intrusion, which has been categorized as normal and abnormal data have been, in turn, displayed by TP and TN. Uncategorized normal and abnormal cases have been, in turn, depicted by FP (False Positive) and FN (False Negative).

TP has been found to be a term employed in educational settings that refers to a network's accuracy. Conversely, FN (false negative) occurs once the model incorrectly identifies. Similarly, FP happens once the model mistakenly classifies a healthy image to have a stone. Finally, TN represents that the classifier correctly identifies an image without a stone as healthy. This approach can effectively optimize the architecture of a DBN and can ascertain the overall network configuration and the depth of hidden layers.

A DBN consists of a restricted Boltzmann machines and backpropagation neural network. If RBM is utilized, the restricted Boltzmann machine forms a two-layer neural network with a hidden layer and an input layer, allowing direct connections among nodes within the identical layer. During the DBN training process, the input data has been initially taken from the bottom layer, then it is gradually increased through RMB layers to gather information for the hidden layer, which serves as input for the subsequent model. the hidden layers have been composed of RMB, which has been represented as d^{th} layer and hidden layers, hd. it should be noted that d is between 1 and n.

Num (h_d) shows the quantity of nodes within the current layer. A DBN consists of an input layer, an output layer, and a specific number of neuron nodes within hidden layers. The number of attributes indicates the number of nodes in input layer, and the entire quantity of data classes indicates the number of nodes in output layer. Within the current study, an enhanced algorithm is employed, called DDMO to optimize the structure of the network with the purpose of ascertaining $num\ (h_d)$ and quantity of hidden layers.

3. Dynamic Dwarf Mongoose Optimization Algorithm

The optimization approach has been developed, and the structure of the current algorithm has been provided below.

3.1. Inspiration

Animals strive to inhabit areas characterized by useless trees, numerous termites, and rocks. Such habitats can be found in the semi-deserts of Africa and bush areas of Savannah. The dwarf mongoose is Africa's smallest predator, with a body length of approximately 47 cm. While the weight of adult individual varies, myriad experts believe it to be around 400g. They typically reside in family groups that are led by a female and a pair of alpha individuals who guide the others.

The number of female individuals exceeds the number of males, and there are more young individuals than older ones. What makes these animals particularly fascinating is their level of generosity and cooperation, especially when compared to mammals. They work together in various tasks, such as babysitting, guarding, intruding, and hunting, which

are divided based on gender and age. There is a wealth of published information available about these individuals, covering aspects like relationships, their roles, and rank order diversity within the group.

These individuals use their anal glands and cheek to detect vertical or flat objects in their surroundings. Once they identify something, they get more confident and ensure that they are not threatened. The extent of marking varies based on the priority ranking of the group; moreover, it should be noted that these individuals collaboratively mark the zone. Reports indicate that their habitat covers a vast region in the Taru Desert, characterized by an abundance of termites, numerous useless trees, and rocks. One particular family spends 22 days marking all the objects in their region. This study suggests that size of family reflects various factors, such as the exploration, use of sleeping hills, and rate of coverage.

As time goes by, this individual can improve the elements associated with their family size, such as exploration, use of sleeping hills, and rate of coverage. They target the eyes of their prey so their bite does not kill, which is why they are not able to hunt larger creatures. The social manners and ecological adaptation of these individuals have been influenced by their method of catching prey. This animal has two main adaptations, which are as follows:

- **Size of Target, Dimension of Group and use of Space**

These creatures have a specific way of catching. They only go after preys with small sizes, so they can feed their young. Their usual targets include small birds, arthropods, gecko lizards, and mammals. Due to the widespread and unpredictable food sources of mongooses, they have to search extensively to find a good meal. These animals lead a semi-nomadic routine, which means families have to travel far for hunting and seldom return to the same sleeping hill. By using this approach, they make sure that no area is overhunted, reducing the depletion of prey and ensuring fair hunting across the entire region.

The dominant female emits short nasal calls or vocalizes approximately 2 kHz in order to maintain group cohesion during hunting. The group's hunting range varies based on the dimension of group, potential interference from other predators, and presence of young members. The alpha female leads the foraging process, determining the situation, sleeping hills, and path.

- *Food Supplying*

In these groups, there are no observed instances of feeding behavior amongst lactating females and young individuals. The social structure of these individuals, particularly parenting manner, has influenced the development of compensatory behavioral adaptations described subsequently.

- *Babysitting*

Some individuals, usually a combination of males and females, serve as babysitters. They nurture young individuals by the time the group returns at midday. They do not construct any home for the youngsters; instead, the adults transport them to the resting mounds. The young individuals begin to forage before they are fully developed, and they are unable to run, which hinders the group's foraging capabilities.

To sum up, these individuals cannot effectively hunt large prey. Due to their lack of structured group predating and a deadly bite, mongooses form a society that allows individuals to defend themselves and move in various mounds of sleeping continuously. These animals lead a semi-nomadic life within a sufficiently large region to support one another. Their nomadic manners prevent over-exploitation of a particular region and ensure the global search of the entire zone, as they never return to the same sleeping hill.

3.2. Population Initialization

The first step of the current algorithm is the population initialization of these animals' community (Z), as depicted in the following formula. The population is generated between the UB (Upper Bound) and the LB (Lower Bound) in an automated manner.

$$Z = \begin{bmatrix} a_{1,1} & a_{1,2} & \cdots & a_{1,d-1} & a_{1,d} \\ a_{2,1} & a_{2,2} & \cdots & a_{2,d-1} & a_{2,d} \\ \vdots & \vdots & a_{c,g} & \vdots & \vdots \\ a_{m,1} & a_{m,2} & \cdots & a_{m,d-1} & a_{m,d} \end{bmatrix} \quad (7)$$

where, the current population has been represented by Z that has been produced by the use of the Equation 8. The quantity of individuals is demonstrated by m, the situation of dimension g of the population i has been displayed by $a_{c,g}$, and the dimension of the problem has been depicted by d.

$$a_{c,g} = unifrnd(VarMin, VarMax, VarSize) \quad (8)$$

where, the proportion of the uniform distribution has been shown by $unifrnd$, and the highest and the lowest boundaries have been, in turn, indicated by $VarMax$ and $VarMin$. The quantity of decision variables has been displayed by $VarSize$.

3.3. The Model of Dwarf Mongoose Optimization

The proposed methodology of the current algorithm replicates the behavioral adaptations of these animals. These behavioral adaptations include the scope threshold of the prey, semi-nomadic way of life, babysitters (social structure), and more. The social organization has been categorized into alpha groups, babysitters, and scouts. All group collaborate in adjusting compensatory manners that lead to a semi-nomadic way of life in a large area to meet the needs of every group member.

These animals are well-known for their collaborative behavior, as they collectively search for food and seek out new hills together. The alpha group begins foraging and searching for a novel hill simultaneously. The estimation of the average sleeping mound value for all iterations determines the subsequent phase in the mongoose population that has been shown in Equation 8. Their nomadic behavior prevents overexploitation of a particular area and ensures exploration of the whole region, as they never return to a previously visited hill of sleeping. The process of the current algorithm is presented in three stages in Figure 3.

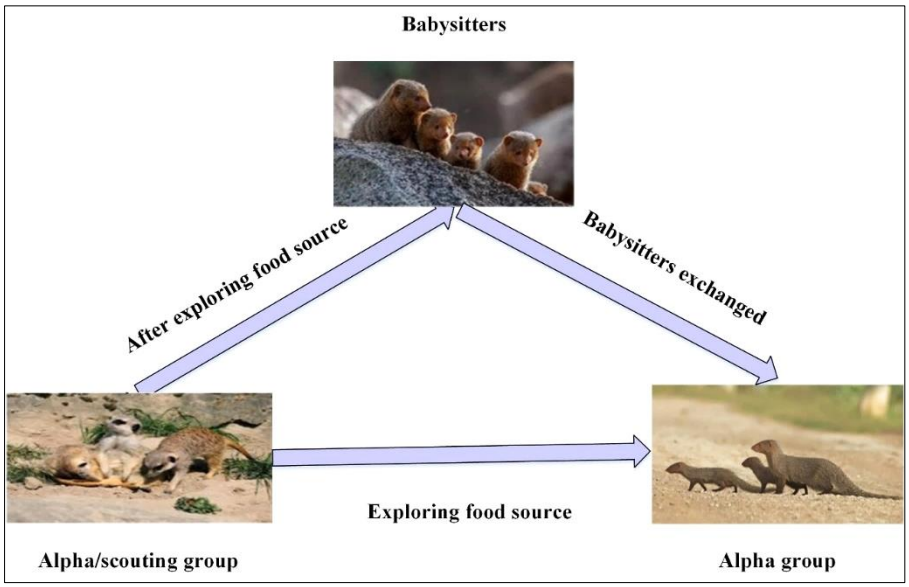

Figure 3. Process of the current algorithm

3.4. Alpha Group

Each objective function of solution is computed once the population have been initialized. the probability of fitness has been computed by Equation 9. Additionally, probability value selects the female alpha (x):

$$Z = \frac{fit_c}{\sum_{c=1}^{n} fit_c} \tag{9}$$

where, Z represents the probability of selecting a particular solution based on its fitness value (fit_c), relative to the total fitness of the entire population ($\sum_{c=1}^{n} fit_c$). The quantity of individuals within group of alpha is equal to $n - b_s$, b_s stands for the quantity of babysitter, the female alpha's vocalization has been demonstrated by $peep$, directing family members, and the prior sleeping hill has been displayed by $\emptyset$. To represent the nutrition situation of an individual, the subsequent formula has been employed:

$$Z_{c+1} = Z_i + phi * peep \tag{10}$$

where, the stochastic proportion has been displayed by phi ranging from -1 to 1, and the hill of sleeping has been illustrated in the following:

$$sm_c = \frac{fit_{c+1} - fit_c}{\max(|fit_{c+1}, fit_c|)} \tag{11}$$

The mean value of the sleeping hill has been calculated in the subsequent manner:

$$\varphi = \frac{\sum_{c=1}^{n} sm_c}{m} \tag{12}$$

Once babysitters are changed and the subsequent sleeping hill or nutrition source is evaluated, the algorithm begins scouting stage.

3.5. Scout Group

The dwarf mongooses are well-known for their habit of not returning to their previous sleeping hill. As a result, a group of scout individuals looks for a novel sleeping hill to facilitate global search. Scouting and foraging activities occur at the same time, influencing the overall performance of these individuals. If these individuals forage over a sufficient distance, they will discover a novel sleeping hill. The equation below illustrates the role of the scout individuals.

$$Z_{c+1} = \begin{cases} Z_c - CF * phi * rand * [Z_c - \overrightarrow{M}] & if\ \varphi_{c+1} > \varphi_c \\ Z_c + CF * phi * rand * [Z_c - \overrightarrow{M}] \end{cases} \tag{13}$$

where, the stochastic quantity has been represented by $rand$, ranging from 0 to 1. The variable that controls collective-volitive movement has been displayed by $CF = \left(1 - \frac{iter}{Max_{iter}}\right)^{\left(2\frac{iter}{Max_{iter}}\right)}$. Moreover, $\vec{M} = \sum_{c=1}^{n} \frac{x_c \times sm_c}{X_c}$ indicates the vector, which can determine the path of the individuals to the new hill of sleeping.

3.6. The Babysitters

The group's subordinate individuals, known as babysitters, consistently rotate their roles in order to allow the mother to direct the individuals in daily foraging. The female alpha typically returns at midday to feed the babies in the evening. The number of babysitters depends on the scope of the population. A decrease in the overall population scope affects the algorithm based on the percentage. The group has been modeled by reducing the population scope represented by the percentage of babysitter. Recently collected data on scouting and food sources, which was held by other individuals, is reset by the exchange of babysitter. The fitness weight of the babysitters has been considered 0, guaranteeing a decrease in the average weight of the alpha group in the next iteration. This will cease the movement of the group and highlight local search.

3.7. Dynamic Dwarf Mongoose Optimization Algorithm

The most recent project involves the implementation of a customized improvement to the current optimizer with the aim of enhancing its exploration capabilities and overall efficiency, specifically for sports image classification tasks. The original Dwarf Mongoose Optimization Algorithm is based on gas solubility principles and utilizes a unique search method to navigate the solution space.

We propose a dynamic iteration of the Dwarf Mongoose Optimization Algorithm to address this limitation. In this iteration, the energy value computation equations are adjusted to include dynamic terms "b" and "c". By incorporating these two terms into the primary formulation, the mathematical expression can be achieved as follows:

$$Z_{c+1} = Z_i + phi * c \tag{14}$$

$$Z_{c+1} = \begin{cases} Z_c - b * phi * rand * [Z_c - \overrightarrow{M}] & if\ \varphi_{c+1} > \varphi_c \\ Z_c + CF * b * rand * [Z_c - \overrightarrow{M}] \end{cases} \tag{15}$$

The dynamic terms are categorized while utilizing functions that can grow over time and have been found to be adjustable to learn time-dependent patterns in this area, thereby improving optimization outcomes.

$$b = \frac{A}{1 + exp(-kt)} \tag{16}$$

$$c = C_0 \times \left(1 - \frac{t}{T}\right)^p \tag{17}$$

where, k stands for the rate of method, and the parameters t, k, and A demonstrate constants that affect the function's shape. The initial value of b is 0 and slightly gets closer to A as t increases. The constants C_0, T, and p can shape the function.

where, the initial value of c is C_0 and can diminish to 0 as t gets close to T. The parameter p can determine the rate of diminish. By utilizing an Enhanced Gas Solubility Optimizer, the system can learn raised adaptability and flexibility to changing circumstances, which can result in better optimization outcomes.

3.8. Algorithm Authentication

The DDMO algorithm was extensively tested and evaluated by using the well-known "CEC-BC-2017 test suite" benchmark, which has come to be recognized as the standard tool for assessing the various optimization algorithms. This benchmark contains 30 different functions that are carefully grouped into categories of multimodal, unimodal, composition functions, and hybrid. The evaluation focused on the solution space ranging from -100 to 100, thus covering the wide range of optimization difficulties. To demonstrate the efficacy and the excellence of the DDMO, its performance was measured against five state-of-the-art optimization methods, which include the Reptile Search Algorithm (RSA) [18], Lévy flight distribution (LFD) [19], Poor and Rich Optimization (PRO) [20], Teamwork Optimization Algorithm (TOA) [21], and Manta Ray Foraging Optimization (MRFO) [22]. Parameters for establishing the algorithm under research are listed in Table 1.

Table 1. Parameter values for the algorithms

Algorithm	Parameter	Value	Algorithm	Parameter	Value
TOA [21]	t	0.16	LFD [19]	Threshold	2
	l, f	0.5		CSV	0.5
	c	0.8		β	1.5
	e	0.2		α_1	10
PRO [20]	p	0.16		α_2	0.00005
	r	0.9		α_3	0.005
	b	0.2		∂_1	0.9
	c	0.8		∂_2	0.1
	m	0.01	RSA [18]	α	0.1
MRFO [22]	S	2		β	0.01
DDMO	b	0→1			
	c	1→0			
	Learning Rate	1e-4			

These parameters, with additional constants that modulate their behavior, were chosen based on empirical testing and tuning. The temporary adaptation of these parameters helps the algorithm learn time-dependent patterns and improves its capacity size in order to optimize complex models such as DBNs. Despite showing better performance than several other algorithms such as Reptile Search Algorithm (RSA) and Lévy Flight Distribution (LFD), it is possible that other optimization approaches might perform better in particular situations. Some algorithms with very fast convergence or specially adapted to solve deep learning problem might outperform the DDMO in many cases. Therefore, considering the sensitivity to hyperparameter settings and DDMO's strong performance for a wide range of optimization problems, DDMO is chosen for improving the DBN model in this research.

The efficiency, convergence behavior, and robustness of DDMO were deeply analyzed by applying it to the same benchmark functions and comparing its performance with established algorithms. The results obtained from this assessment have provided a very useful insight into the strengths and capabilities of DDMO in handling various optimization scenarios.

The efficiency of an optimization algorithm is strongly linked to the proper choice of its parameters, which, in turn, requires an empirical fine-tuning process in order to guarantee the best possible performance. Initialization methods cannot guarantee a globally optimal solution, but they are essential for reaching near-optimal results. Ten runs have been conducted for each function in order to improve the precision of our assessments, gathering data which enabled us to calculate important metrics, including the standard deviation (StD) and the average value (Avg).

Table 2 can provide a succinct comparison of the suggested algorithm's efficiency relative to other approaches, emphasizing the outcomes of metric analyses and extensive simulations. This thorough assessment emphasizes the dependability and robustness of suggested method in overcoming the CEC-BC-2017 test suite.

Table 2. Comparison of the efficiency of the approaches used to investigate the CEC-BC-2017 examination data

Function	DDMO		TOA		PRO		Function	MRFO		LFD		RSA	
	Avg	Std	Avg	Std	Avg	Std		Avg	Std	Avg	Std	Avg	Std
Fl	155.8451	134.1354	432.2068	4.98E+09	3406427	259038.8	Fl	369.4836	5.29E+09	0.834283	1614.217	3188802	295135.1
F3	0.039448	0.033027	0.090196	14276.77	1947.208	14583.99	F3	0.088983	14553.33	63081.25	73011517	1803.963	13804.56
F4	0.159145	0.098433	0.228985	501.9505	285.789	205.5674	F4	0.227215	496.4402	2030.17	680137.6	338.2699	238.6223
F5	1.639752	0.940624	2.38302	275.9343	387.9065	12.38122	F5	2.224378	289.9369	42.6894	3020.441	422.6586	11.51386
F6	0	0	0	438.2158	313.2795	11.26281	F6	0	426.8875	98.64039	12588.33	270.2299	10.10971
F7	1.268358	1.08983	3.212386	479.2958	432.6289	21.32811	F7	3.042086	423.9379	1.619911	1324.89	382.3895	20.61518
F8	1.188366	1.045409	1.866585	529.2849	580.2207	12.41489	F8	1.852949	455.4979	2.460154	1021.737	533.1222	13.27141
F9	0	0	0	1480.007	1251.511	356.9197	F9	0	1598.421	708.1678	2788285	1138.132	411.4834
F10	66.79377	61.17681	105.8914	2065.599	1364.208	172.4444	F10	104.7943	1870.579	87.54662	3392509	1389.759	193.3928
F11	0.334497	0.306493	0.810668	1677.055	442.6748	1900.114	F11	0.680234	1681.794	0.043063	1845.05	478.3558	1841.941
F12	373.5565	196.2201	61611.6	75943000	1943502	1.07E+08	F12	71785.95	77530917	29.01669	1723.929	2192183	99663604
F13	677.3681	521.9732	1841.971	695670.3	11589.36	3502400	F13	1705.634	733625.1	3.747821	1888.977	12714.24	3560503
F14	35.43768	26.10561	39.26453	2846.843	883.6473	2544.933	F14	40.24386	2460.837	1.921157	1612.874	870.669	2193.146
F15	67.1724	63.06558	104.404	14213.86	5470.999	43290.51	F15	116.8766	13772.92	39.69882	1241.358	4892.797	50827.78
F16	1.480911	1.328207	1.956867	1191.091	913.7348	197.086	F16	1.904508	1297.846	8.741904	2502.923	851.9899	182.0661
F17	1.144434	0.952313	2.421654	936.6349	1235.5	53.83381	F17	2.665462	905.4298	26.63612	2220.269	1292.293	47.89963
F18	392.4904	285.7467	722.8176	2841241	12907.71	643.2046	F18	768.5636	2538601	1.281572	1627.155	12999.02	731.0223
F19	99.25805	76.95837	83.74941	2839642	36035.06	897.2253	F19	86.05846	3401427	40.98675	2241.484	31773.18	964.9777
F20	0.025549	0.0187	0.042709	1981.783	1318.833	57.56275	F20	0.042703	1779.529	12.02758	1973.584	1263.453	57.78153
F21	17.98472	11.28371	26.76413	1800.345	1754.131	29.36836	F21	26.08687	1961.339	9764.337	3235.239	1810.41	27.0417
F22	1.72117	1.081444	3.278282	1974.357	978.0655	474.9366	F22	3.82203	1804.575	20.15	11.089	1025.917	470.7445
F23	2.180832	1.663129	1.743687	1757.292	1378.614	14.87866	F23	1.864888	1553.183	0.834283	1614.217	1630.361	16.10373
F24	14.21901	9.078791	42.52746	1311.768	2071.978	18.89791	F24	44.58316	1245.385	63081.25	73011517	1778.898	18.96341
F25	7.581974	6.431415	9.243752	2537.538	1577.852	175.3691	F25	9.783657	2298.909	2030.17	680137.6	1573.804	172.9787
F26	28.21773	26.97241	27.03634	2248.974	2383.648	248.0414	F26	27.27381	1891.702	42.6894	3020.441	2488.486	231.9842
F27	0.54227	0.485246	1.124073	1727.474	1353.523	45.33441	F27	1.283852	1640.537	98.64039	12588.33	1471.503	39.36161
F28	26.01248	19.27747	39.02323	1868.218	1474.3	61.19412	F28	44.98857	1880.525	1.619911	1324.89	1567.028	65.97452
F29	8.804995	6.515521	10.94469	2169.397	2875.506	133.6926	F29	11.93978	2212.036	2.460154	1021.737	2577.259	135.0621
F30	571.1705	287.593	10406.98	3385.507	2980265	130583.7	F30	10040.09	3323.112	708.1678	2788285	2908302	119686.9

DDMO has the best average values among the compared algorithms in all functions, which means that DDMO yields better solutions. Besides, DDMO has lower standard deviation values, which means that it is more stable and reliable, especially for functions F1, F3, F4, F5, F7, F8, F11, F14, F15, F17, F19, F20, F21, F23, F24, F25, F27, F28, and F29. Even though some algorithms surpass other optimizers in particular functions, the entire consistency and effectiveness of DDMO across the test suite represent its capacity for reliability and robustness as an optimization tool. These findings underpin DDMO's capability in handling a wide range of optimization challenges, hence placing it as a promising solution for real-world optimization problems.

4. Research Methodology

4.1. Problem Statement

In maintenance environmental standards and operational efficiency, the monitoring of noise levels at substations holds significant importance. Taking into account a typical substation situated in a diverse geographical setting, where a variety of electrical device such as reactors and transformers are in use. The wide-ranging situations of National Grid substations, which are between urban areas and mountainous terrains, pose a distinct challenge in the management of potential noise disturbances. Therefore, we advocate for a dual-pronged strategy for an innovative noise monitoring system tailored specifically for National Grid substations:

Initially, the system is designed to incessantly gather data of noise at the borders of substations, utilizing real-time analytics to promptly identify and notify in case noise levels exceed predetermined pollution thresholds. This ensures timely detection of potential noise pollution occurrences.

Subsequently, the system transcends mere detection by integrating root-cause analysis capabilities. By making use of the gathered noise data, the system strives to pinpoint the specific type of equipment responsible for heightened noise levels. This crucial information enables operation and maintenance teams to promptly address the source of noise pollution, thereby facilitating effective and targeted interventions. The proposed system for monitoring substation noise is structured with a layered architecture, as illustrated in Figure 4.

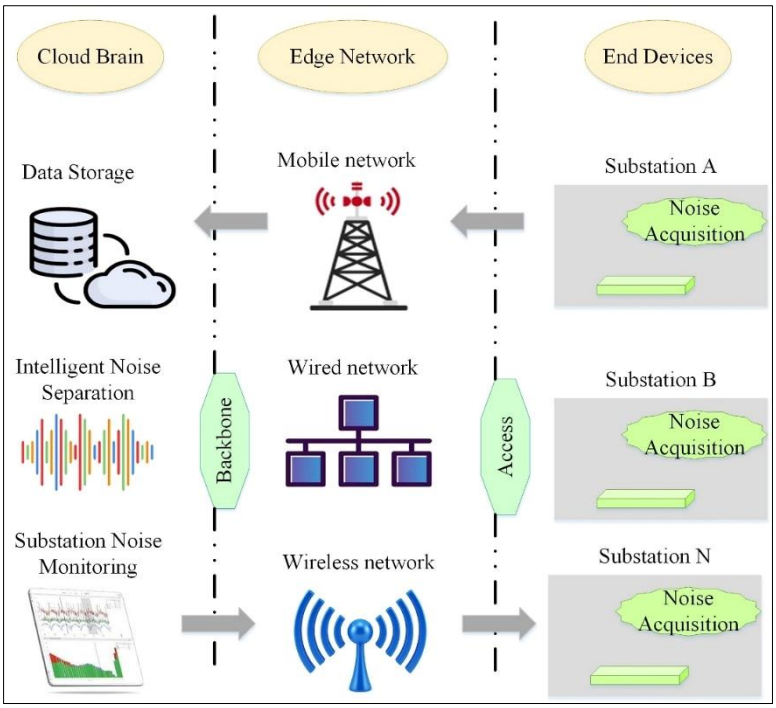

Figure 4. Comprehensive structure of the substation noise monitoring system

It comprises 2 major elements:

- Noise Acquisition Devices (Terminal Layer): This layer involves the installation of specialized devices strategically placed within the substation to collect noise data. These include advanced sensors and processors that make accurate and continuous noise measurements. This system processes and analyzes sound data directly to avoid unnecessary data transmissions and delays in communication. It calculates various variables, such as different frequency weightings pressure levels of sound, time-weighted pressure levels of sound, and octave from the sound data obtained. The device detects anomalies based on these calculations. After the occurrence of an anomaly, the data from one-minute audio and outcome will be transferred to the data center of the cloud for further investigation and keeping of records.
- Cloud Layer (Data Visualization and Noise Analysis): This layer involves sophisticated algorithms that analyze the noise data collected. It involves real-time processing, analysis of historical data, and advanced analytics for anomaly detection, pattern recognition, and actionable insights. It also provides tools for data visualization to interpret noise trends, monitor regulatory compliance, and make informed decisions. The main goal of this research is the proposal of an efficient deep learning approach using the enhanced Deep Belief Network to accurately identify electrical equipment noise amidst environmental noise. This method can significantly improve the accuracy of noise monitoring and enable early fault detection. Moreover, for better visualization of the noise monitoring results, the new system will be able to visualize results in a monitoring management platform that will enhance both the interpretation and visualization of the noise data collected.

4.2. Device for Self-Generated Noise Collection

A self-developed noise collection device refers to a piece of equipment tailored or made in-house for capturing and measuring noise. In the substation noise monitoring system, this device would be adjusted to meet the specific needs of National Grid substations. A summary of the components that may be involved in a self-designed noise collection device is outlined below.

- Customized Hardware: Specialized microphones or sound sensors could be installed on the device, which will measure noise data more precisely at various frequencies related to the substation environment. It can include measuring equipment designed to withstand harsh conditions of changing temperatures, exposure to weather, and electrical interference.

- Data Acquisition and Processing: Initial data processing, including amplification, filtering, and analog-to-digital conversion, would be possible because of onboard processing capability. In this way, captured noise signals are converted to useable digital data that may be further analyzed.
- Communication Interface: This device would have a communication interface to send the captured noise data to the cloud or a central server over wireless connectivity (Wi-Fi, cellular, or satellite) or wired Ethernet for storage and advanced analysis. Real-time data transmission allows for timely detection and alerts.
- Power Source: Since some substations are located in very remote areas, the device should be able to run using an integration of grid electricity and renewable energy sources, along with backup batteries for continuous operation in case of power outages or grid failures.
- Enclosure and Mounting: It will be designed such that it protects the internal parts of the device from the environment while ensuring optimum capture of noise. Some mounting options include poles, walls, or customized structure mounts near substation boundaries for wider coverage of areas.
- Calibration and Maintenance: Noise acquisition would involve undertaking regular calibration and maintenance tasks to keep network's reliability and accuracy. For example, it would undergo periodic checks, cleaning, and adjustments to ensure data integrity throughout the process.

The National Grid improves noise monitoring by developing a self-sufficient noise acquisition device, which allows for tight control over the required specifications and customizations. This approach ensures a bespoke solution that integrates smoothly with their current infrastructure.

4.3. Noise Separation Based on the Proposed DBN/DDMO

The evaluation of noise properties in substations covers both internal equipment noise and external environmental interference. The main sources of equipment noise within substations are corona noise, reactor noise, and transformer noise. However, the analysis of corona noise, which originates from charged structures, is affected via the predominant noise from reactors and transformers. Hence, noise of corona has been acquired via controlled laboratory replications of corona discharge. To effectively monitor noise pollution in substations and accurately differentiate between equipment noise and environmental noise, a noise separation procedure that has two stages is developed, as shown in Figure 5.

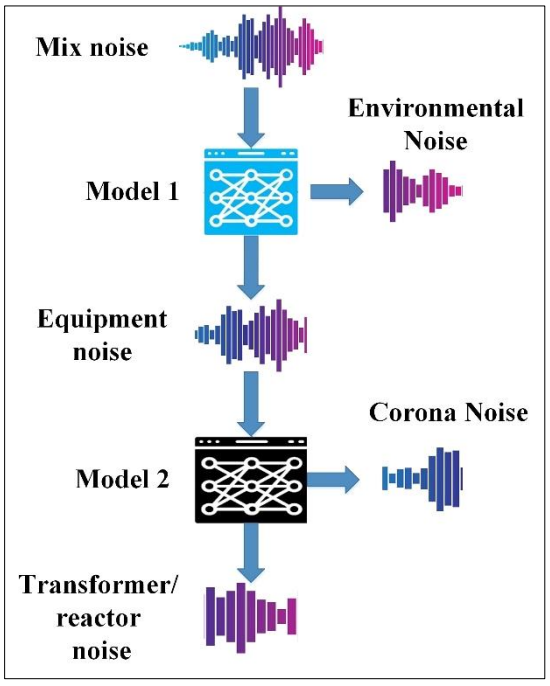

Figure 5. The visual representation of the noise separation process in two steps

The model's input reflects real-world situations by including a combination of reactor noise, transformer noise, environmental noise, and corona noise. Initially, the proposed DBN/DDMO model is utilized to distinguish between substation equipment noise and environmental noise. This initial separation enables the detection of noise levels that surpass standard limits. If the noise in the substation exceeds the set threshold, further analysis is required. The second step involves separating various types of substation equipment noise. Because of the similarities between reactor noise and transformer, they have been classified as the same kind of noise.

Through this secondary separation, the precise machinery generating the high levels of noise is then identified. This two-step procedure aids in monitoring overall noise pollution and in formulating focused noise mitigation strategies by recognizing sources of excessive noise within the substation environment.

The evaluation of noise separation optimizers in the substation noise monitoring system relies on a recently established dataset specifically for this purpose. The raw data needs to be pre-processed to train the model properly in order to differentiate between environmental noise and equipment noise. The raw data can be obtained from [4].

Noise separation algorithms will be evaluated on a very elaborately prepared dataset mimicking the complex noise at substation environments. An ideal representation of equipment noises will be achieved by integrating the noise of transformer and reactor. This combined equipment noise will be mixed with miscellaneous ambient noises like insect-generated and human talking, birds chirping to represent the elaborate mixture found in actual substation surroundings in an intricate manner.

This multi-step mixing process effectively can capture the overlapping and varied features of the noise sources. The resultant dataset forms a solid basis to appraise the efficacy of the noise separation optimizers. Through detailed analysis, thorough assessments of this diverse dataset can be achieved with respect to model performance across various experimental scenarios that ensure precision and dependability in real-world substation noise monitoring applications.

4.4. Implementation of Sound Level Algorithm

4.4.1. Time Weighting Design

Time weighting design provides an important impact in sound level measurement by enabling the analysis of noise variations over time. Different time weightings, such as Fast (F), Slow (S), and Impulse (I), are utilized to capture rapid fluctuations, long-term trends, and impulsive noises, providing a comprehensive understanding of sound level dynamics. This research utilizes Fast time weighting, which is designed to quickly respond to changes in sound levels, making it suitable for detecting short-duration events or rapid fluctuations. Fast time weighting is often used for measuring peak or maximum sound levels, with a time constant typically set to a small value for a rapid response to changes in the input signal. The formula for Fast time weighting is presented as follows:

$$FTW = 20\log_{10}\left(\frac{P}{P_0}\right) - 2.5\log_{10}\left(\frac{T}{T_0}\right) \tag{18}$$

The sound pressure of input signal has been represented by P, whereas the sound pressure of reference has been illustrated by P_0 (usually 20 μPa). Fast weighting has been described via the time constant T, and the time constant of reference is demonstrated through T_0 (typically 1 second).

It offers the user the choice between Fast, Slow, and Impulse time weighting for various monitoring needs. The user-defined time weighting is used for computation of the sound pressure level, thereby giving an individualized response to a variety of noise attributes. This flexibility enables a fine-scale analysis of the ambient noise and allows users to effectively recognize and solve a wide range of sound level issues.

4.4.2. Frequency Weighting Design

Frequency weighting is a fundamental part of sound level measurement and analysis, as it considers the nonlinear way in which the human ear perceives loudness. Different frequencies of sound are perceived differently, and frequency weighting curves are used to simulate this auditory effect. The A-weighting curve is the most commonly used frequency-weighting curve because it is specifically designed to reflect the sensitivity of human hearing to different frequencies. The A-weighting curve has been mathematically formulated as follows:

$$A - weghting = 20\log_{10}\left(\frac{P}{P_0}\right) + A(frequency) \tag{19}$$

where, P represents the sound pressure of input signal, P_0 demonstrates the sound pressure of reference (usually 20 μPa), and A(frequency) has been found to be the frequency-dependent adaptation in decibels (dB) that is demonstrated subsequently:

$$A(frequency) = \begin{cases} 0, & for\ frequencies\ below\ 1\ kHz \\ \frac{1}{2}(1 - \cos(\pi \log_2 frequency)), & for\ frequencies\ between\ 1\ kHz\ and\ 2\ kHz \\ 2(frequency - 2000), & for\ frequencies\ above\ 2\ kHz \end{cases} \tag{20}$$

This equation provides a modification in the sound pressure level with respect to frequency, where lower frequencies are less attenuated and higher frequencies experience a more significant reduction.

The sound level algorithm includes an A-weighting curve that helps measured sound levels align with the human auditory perception. This is achieved by applying the aforementioned equations in the computation of the pressure levels of sound. By incorporating the A-weighting curve, the algorithm delivers sound levels that are closer to the human experience of loudness, hence increasing the applicability and interpretability of the data for noise monitoring initiatives.

5. Simulation Results

The noise monitoring system, consisting of three major components-a noise monitoring device, a sound source, and a platform of web display-was tested in the test platform in [4]. The sound source consisted of a signal generator, a computer, and a dodecahedral sphere speaker, which provided regular sound distribution. The computer controlled the generator of signal to develop various signals with varying frequencies and amplitudes, which were then passed to the sphere speaker.

These sound signals were recorded by a noise monitoring device, which converted the signals into digital data, performing real-time frequency-weighted and time-weighted SPL (Sound Pressure Level) calculations, as well as octave analysis. Conforming to the international standard IEC 61672 for Class 1 sound level meters, the device forwarded the results to a backend database over a 4G network to allow for remote access by the platform of web display. The study uses a relatively big dataset of 10,000–15,000 Audio samples of 3 seconds, with 48 kHz sampling rate for different SNRs for diverse coverage. In addition, the incorporation of diverse types of noise in an environment with substation equipment suggests that the proposed system could be adapted to other substation systems as long as the dominant noise characteristics were similar. The model might perform well (>90%) in urban areas (where the acoustic characteristics are more similar to the training set), and potentially poorly (~75% or less) in rural/mountains with different acoustic conditions (e.g., much higher background noise). Figure 6 shows the platform used for the noise monitoring system testing.

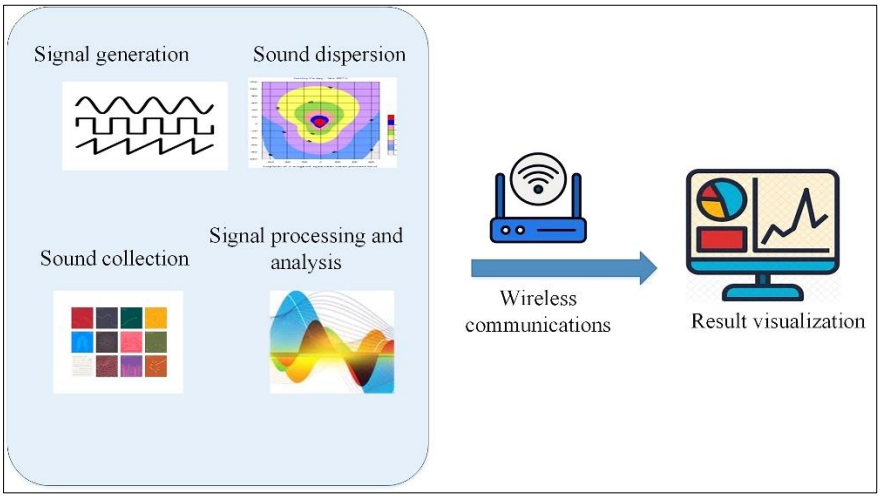

Figure 6. Platform employed for examining the system of noise monitoring

To verify the accuracy of the noise monitoring device, it was subjected to thorough testing in an anechoic chamber, where its capabilities in frequency weighting, time weighting, and octave analysis were scrutinized. This extensive test platform allowed for a comprehensive evaluation of the system's overall performance and the confirmation of the device's precision in practical noise monitoring applications.

5.1. Time Weighting Test

Tests of time weighting are designed to measure the speed of change in pressure level of sound and to check that it meets certain requirements. The system’s response is measured by switching off a continuous 4 kHz sine waveform. Figure 7 represents the sound pressure level using frequency weighting over time for Fast (F) and Slow (S) time weightings, the level of detail is important and allows for monitoring of F and S time weightings to determine how the weightings respond to sound level changes.

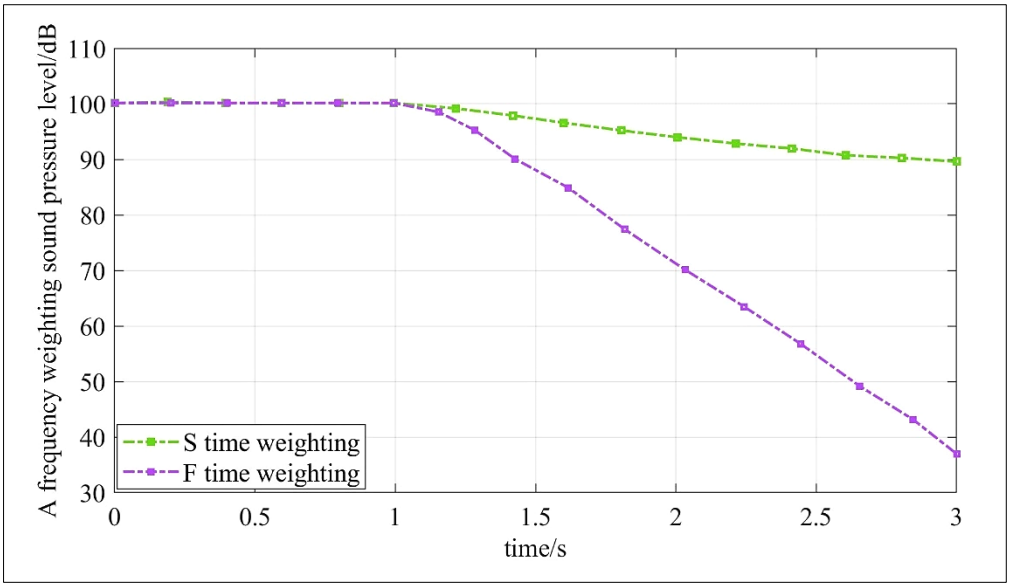

Figure 7. Pressure level of sound with frequency weighting over time for *F* time weighting and *S* time weighting

The solid line is the Fast (F) time weighting, which has a much faster response to sound pressure level changes. Hence the sharper drop in sound pressure after the source is turned off. The device is responding well, with very short time constant (mean 125 ms), resulting especially sensitive to short noise events like equipment glitches or environmental disturbances like chirping birds and human activity. The other dashed curve is for Slow (S) time weighting, which will have a slower return to lower sound pressure levels because it has a longer time constant (1 s). A slower response smooths out the rapid fluctuations, providing a better picture of overall noise level over time.

However, over time the differences between the curves become quite pronounced, and serve to illustrate the differences in the temporal sensitivities inherent to the two weightings: both curves are began at roughly the same sound pressure level (~100 dB), but the dBA curve drops steadily while the dBC curve remains higher with increased time. The temporal weighting approach, however, can diverge considerably depending on how noise is weighed with respect to time, with implications for analyses that are aimed at monitoring noise pollution, with Fast (F) being sensitive to transient phenomena and Slow (S) more sensitive to long-term noise trends. For example, the Fast weighting may be relevant for substation noise monitoring, allowing it to respond to short-duration noise events associated with equipment malfunction or abrupt changes in the surrounding environment in order to facilitate early treatment.

On the other hand, the Slow (S) weighting gives a more filtered view of noise for regulatory purposes to prevent disruption to neighbors, used and modeled by novel statistics such as the time-weighted readings, precise measurements, and time-integrated readings, which provide complementary insights into the noise dynamics in substations. With the F and S weighted incorporation for measurements, the noise level can be verified correctly from substation equipment even in the presence of background noise. This alternating method mirrors the two-step approach of noise separation, as transient noise events can be first detected, and in a second step, a more detailed analysis of sustained noise sources can be conducted, leading to strategies for predictive maintenance and increased substation operational reliability.

5.2. Test of Frequency Weighting

The frequency weighting assessment of the device, which tries to monitor noise, concentrates on making accurate evaluations considering a wide range of frequency between 20 Hz and 20 kHz. Figure 8 illustrates the diversity in amplitude as a frequency function for the custom-made device developed for frequency weighting.

The horizontal axis represents the range of frequency between 0 Hz and 12,000 Hz, and the vertical axis shows the amplitude variance in decibels (dB). The chart has three lines, including a solid line that shows the variance in comparison with the standard curve and two dashed lines indicating the maximum and minimum satisfactory amplitude variances. The continuous line represents little deviation and well within the lines marking the upper and lower limits. This, in essence, validates the accuracy of the bespoke device across the entire tested frequency range and affirms capability of device in measuring noise levels for frequencies between 20 Hz and 20 kHz with very high accuracy in frequency weightings while noise monitoring. This kind of precision is critical for applications requiring accurate noise assessments over a wide range of frequencies.

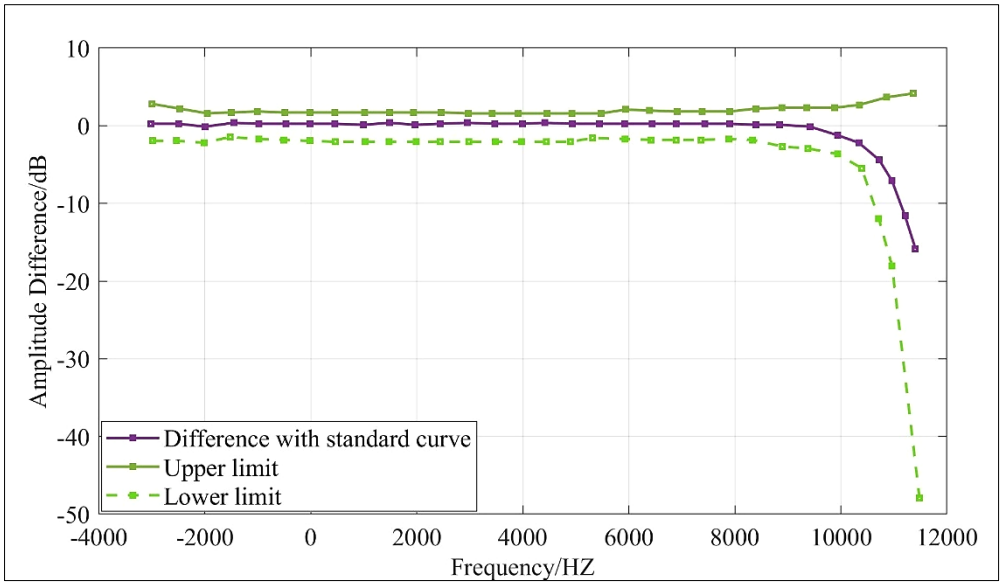

Figure 8. The diversity in amplitude as a frequency function for the custom-made device developed for frequency weighting

5.3. Measurement Indicators

Noise separation algorithms usually involve evaluating the SDRi (Signal-to-Distortion Ratio Improvement) or the SI-SNRi (Scale-Invariant Signal-to-Noise Ratio Improvement) metrics. SDRi calculates the improvement of the SDR from the original noisy signal toward the enhanced signal after the separation of noise. The SDRi formula is given below:

$$SDR_i = SDR_{enhanced} - SDR_{noisy} \tag{21}$$

where, $SDR_{enhanced}$ demonstrates the signal-to-distortion ratio of the enhanced signal, while SDR_{noisy} represents the ratio of the signal-to-distortion of the initial noisy signal. SDR_i represents precious data in terms of the efficacy of the optimizer in minimization of artifacts and distortions caused by the noise.

On the other hand, it has been found that SI-SNRi is a scale-invariant model of the conventional SNR measure. It measures the improvement in the signal-to-noise ratio without being affected by the overall gain or scaling of the signals. The expression of the SI-SNRi is as follows:

$$SI - SDR_i = 10\log_{10}\left(\frac{\|s\|^2}{\|e\|^2}\right) \tag{22}$$

The objective signal has been represented via s, whereas the residual noise has been demonstrated via e. $SI - SNR_i$ has concentrated on the relative improvement of the desired signal's quality compared to the level of noise, making it a reliable performance metric for assessing noise separation optimizers. By including both SDR_i and $SI - SNR_i$, which have been found to be harmonizing evaluations metrics, it is possible to thoroughly evaluate the precision and performance of the suggested noise separation optimizers.

SDRi informs about the decrease of distortions, while SI-SNRi evaluates the improvement in signal quality compared to the level of noise. These two metrics together give a full picture of how well the optimizers perform in enhancing the desired signal and reducing unwanted noise interference.

5.4. Comparative Analysis

5.4.1. Training and Test Analysis of the Networks

We have made a thorough comparison between the proposed DBN/DDMO and two other related works, namely AlexNet [11], CNN-VGG19 [12] to show the efficiency of the model. These algorithms have been trained using a carefully constructed dataset in order to improve their noise separation capabilities. A unique loss function that is the negative of SDR_i has been used in order to make sure the accuracy of the sound pressure level of separated noise.

The training procedure has been precisely developed for optimizing the efficiency of these optimizers. It has 200 epochs and an initial rate of learning of 1e-4. In order to adapt to the training dynamics, the learning rate is dynamically adjusted. Specifically, once the accuracy of the validation set remains unchanged for 3 sequential iterations, the rate of learning gets halved. This adaptive learning rate mechanism ensures that the algorithms can effectively converge without getting stuck in suboptimal solutions. In Figures 9 to 11, we can see how the training and validation loss change over time for the proposed DBN/DDMO, AlexNet, and CNN-VGG19.

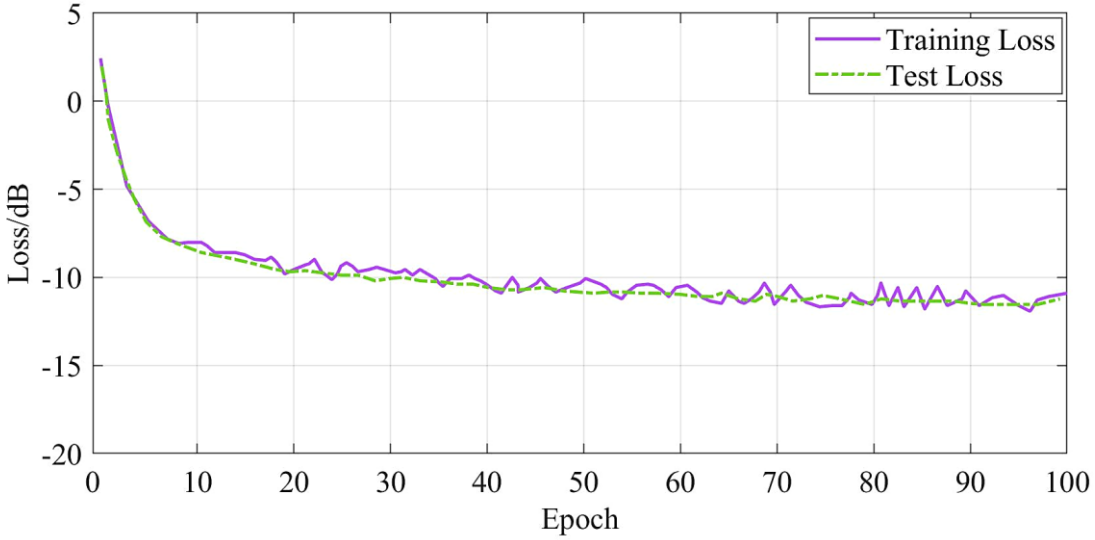

Figure 9. Training and test loss versus the number of epochs for the proposed VGG19

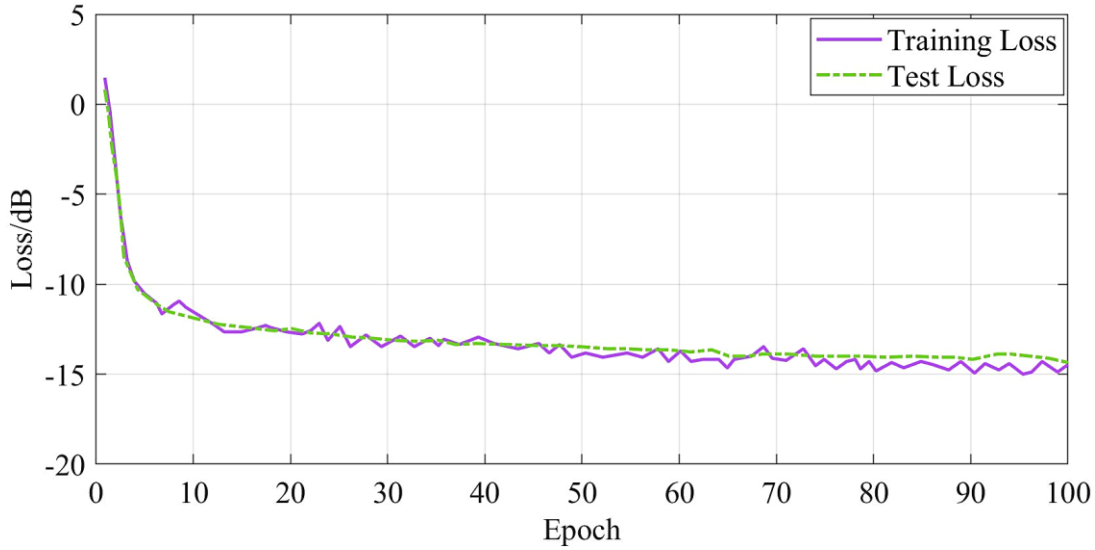

Figure 10. Training and test loss versus the number of epochs for the proposed AlexNet

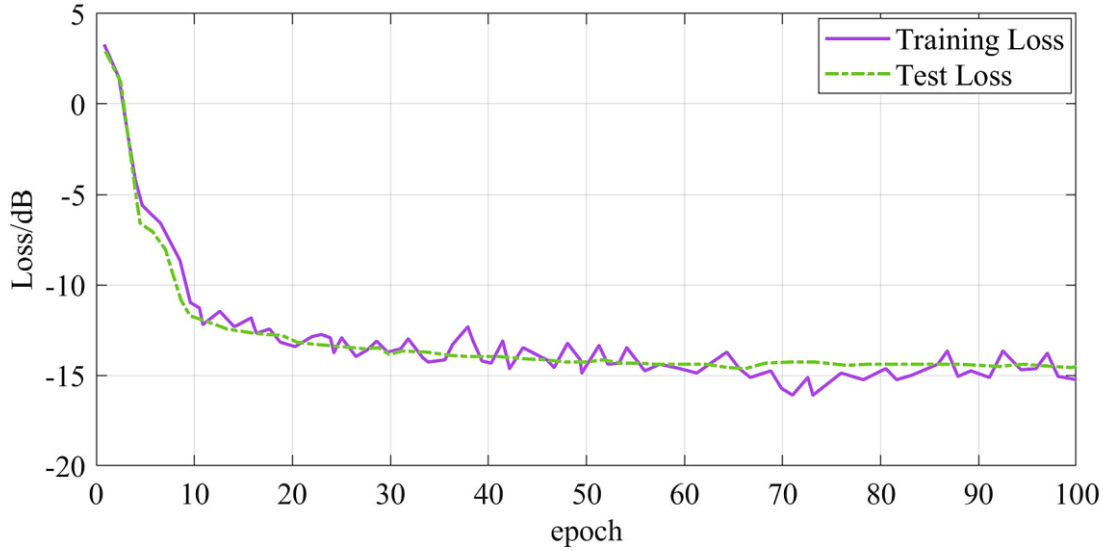

Figure 11. Training and test loss versus the number of epochs for the proposed DBN/DDMO

The DBN/DDMO, AlexNet, and CNN-VGG19 models show fast convergence in about 28, 18, and 18, respectively training rounds. Although there are some small ups and downs in the later rounds, the general pattern is a steady decrease towards convergence. In particular, DBN/DDMO, AlexNet, and VGG19 have losses that converge to around −11.22 dB, −14.35 dB, and −14.57 dB, respectively. The model chosen for the final test set is determined by the epoch with the lowest loss in the validation dataset.

5.4.2. Performance Analysis

Before we provide the results of the DBN/DDMO, AlexNet, and CNN-VGG19 on the test dataset, let's check out Figure 12. The test dataset includes 600 audio samples, each containing a mix of random environment noise and substation equipment noise like human voice chirping of bird, and chirping of insect. These samples have varying signal-to-noise ratios, last for 3 seconds, and have a sampling rate of 48 kHz.

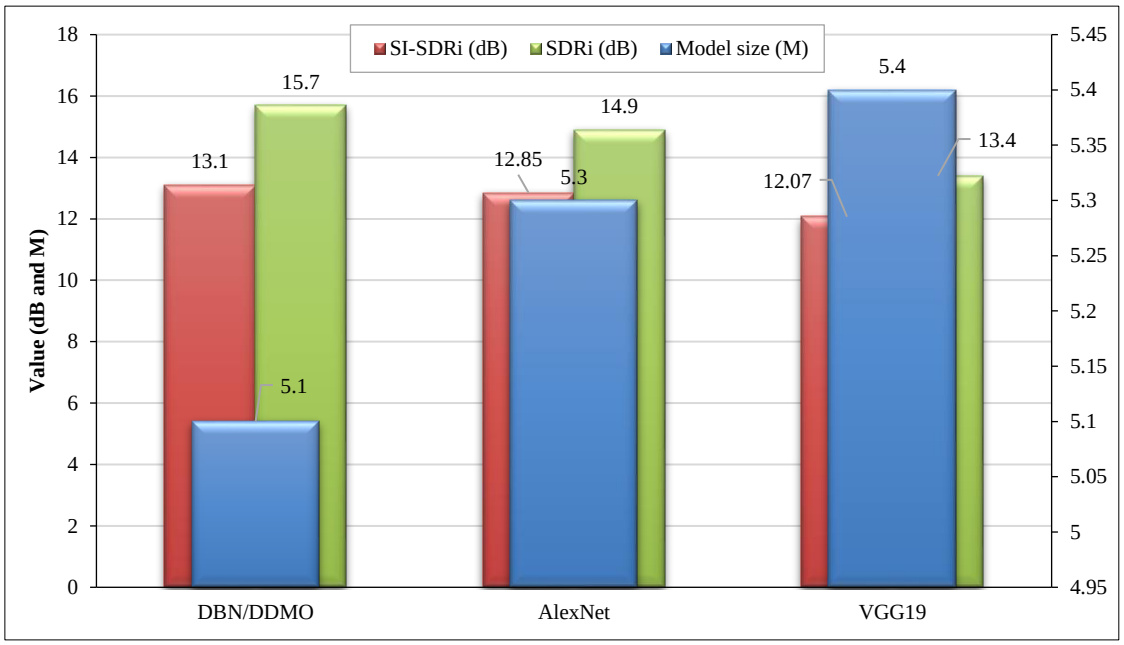

Figure 12. Assessment of the effectiveness of diverse methods in segregating data within the test dataset

As can be observed, the DBN/DDMO model, with a size of 5.1 M, stands out as the top performer among the three models, achieving the highest values for SI-SDRi (Signal-to-Interference ratio improvement) and SDRi (Signal-to-Distortion ratio improvement). It records an SI-SDRi of 13.1 dB and an SDRi of 15.7 dB, showcasing its exceptional capability in isolating substation equipment noise from background noise. The larger value of SDRi verifies that DBN/DDMO can minimize distortion throughout the separation procedure. It is closely followed by AlexNet with a model size of 5.3 M, achieving an SI-SDRi of 12.85 dB and an SDRi of 14.9 dB.

While its efficacy is marginally lower compared to DBN/DDMO, it still shows quite a remarkable ability to differentiate between target noise and background noise. The SDRi value indicates that there is indeed some distortion being introduced by AlexNet, but it is somewhat well-managed. VGG19 is the largest model, with 5.4 M, and shows the least efficacy among the three; It has an SI-SDRi of 12.07 dB and an SDRi of 13.4 dB. VGG19 is comparatively poor, despite its better performance in the substation equipment noise separation task, although quite good for substation noise separation tasks. This lower SDRi shows that this VGG19-based approach will lead to higher levels of distortion, therefore influencing entire quality of the separated noise signals.

5.4.3. Discussions

Maintaining the separation of the noises to three kinds of noises: mechanical, electrical, and environmental, the DBN/DDMS model can enable the filtering of those noises into two steps, top-down and bottom-up (DBN/DDMO). The first step is that the model classifies the substation equipment noise (transformer, reactor, etc.) and environmental background noise, and this is accomplished by identifying the patterns and features by using the model to learn deep representation. Specifically, it is accomplished during training, because the model has seen thousands of hours of mixed audio, with both equipment noise and environmental noise to learn the spectral and temporal nature of those types of noise. Then, in final step, the system specifically identifies equipment types, even between transformer and reactor, with the same characteristics, but distinguishes laboratory corona noise from laboratory duplicates. The separation using the Dynamic Dwarf Mongoose Optimization (DDMO) algorithm optimizes the DBN architecture to minimize all the

distortions and artifacts that can ensure successfully separating the signals from both sources. Using frequency weighting, time weighting, and octave analysis in conjunction with the noise acquisition device allows for real-time differentiation of noise sources and precise calculations of sound pressure levels, thus ensuring accurate identification of noise sources even in complex environments that are typical to substations.

Because of its end-network-cloud architecture, which centralizes data collection, analysis and management, the proposed system shows promise for scaling to large substations or multi-site deployments. Therefore, the availability of a low-cost self-designed noise acquisition devices coupled with the powerful detection capability of deep learning model (DBN/DDMO) fulfills the requirement of modular deployment of the proposed system, where new devices can be added at additional locations and integrated into already existing design. But it's not without caveats when it comes to widespread use. Noise acquisition systems may require specific microphones, processing hardware, and communication solutions that may drive up costs and introduce logistical challenges, particularly in remote or harsh environments.

Also, the cloud specific resources are required to store, process, and analyze large amounts of data in a real-time manner since several substations would produce a significant amount of data. Also, in limited connectivity areas network bandwidth and latency can be real issues that lead to the system being less responsive and reliable. These limitations could be resolved with optimized data transferring protocols, preliminary processing through edge computing and provision of scalable resources on cloud for successfully deploying large scale systems.

The integration of dedicated noise acquisition devices and advanced deep learning algorithms, like the DBN/DDMO model, supports the real-time performance of the system in processing and analyzing noise data. It allows efficient frequency-weighted and time-weighted Sound Pressure Level (SPL) computations, and octave analysis at the terminal layer without the need to transfer huge amounts of unnecessary data. But, throughout data transmission to the cloud for advanced analysis and storage, and if the computer is implemented in a remote substation with limited communication availability, some latency can emerge from the communication interface. Although the system exhibits fast convergence and accurate noise separation, any delays in data transmission or processing in the cloud will have a minute impact on the timely detection of anomalies. Nevertheless, the impact of noise events on system performance can be minimized through various noise reduction techniques, such as frequency filtering and component isolation, improving the system's reliability and robustness.

6. Conclusion

The new system presented in this study is based on deep learning techniques and represents a significant advancement in substation noise monitoring and analysis. Since reliable substation operation plays an essential role in maintaining power supply stability, effective noise monitoring is critical to achieving this objective. Substation equipment noise can be distinguished from interfering environmental background noise through the use of a customized noise acquisition device combined with an enhanced DBN-based noise separation algorithm. The optimized DBN model, further improved using a dynamic model of the Dwarf Mongoose Optimization algorithm, demonstrated promising performance compared with traditional approaches, particularly in terms of scale-invariant signal-to-noise ratio improvement and signal-to-distortion ratio. The deep-learning-based separation algorithms efficiently isolate substation equipment noise, enabling accurate anomaly detection, which may contribute to the implementation of predictive maintenance techniques. The evaluation of the proposed system under different scenarios confirmed its effectiveness and robustness. The data collected after noise separation exhibited regular variations in sound pressure levels, thereby validating the reliability of substation noise measurements even after the removal of disruptive background noise. This study highlights how the integration of dedicated hardware with advanced deep learning methodologies can enhance noise monitoring and analysis in critical infrastructure. Furthermore, the capability for remote noise management and assessment through an end–network–cloud architecture improved noise control and supported timely decision-making. The system contributes to the early detection of equipment faults by accurately identifying abnormal noise levels, thereby preventing sudden failures and enhancing overall substation reliability. This research demonstrates the practical application of artificial intelligence in solving real-world problems and paves the way for future studies on intelligent noise monitoring and predictive maintenance systems for critical infrastructure.

7. Declarations

7.1. Author Contributions

Conceptualization, X.C.; methodology, X.Z., J.W., and X.C.; validation, L.Y. and D.Z.; formal analysis, J.W. and X.C.; investigation, X.C.; data curation, X.Z., J.W., and X.C.; writing—original draft preparation, X.Z., J.W., X.C., L.Y., and D.Z.; writing—review and editing, X.Z., J.W., X.C., L.Y., and D.Z. All authors have read and agreed to the published version of the manuscript.

7.2. Data Availability Statement

The data presented in this study are available on request from the corresponding author.

7.3. Funding

This work was supported by State Grid Corporation of China Headquarters Management Technology Project (Project code: 5200-202318134A-1-1-ZN).

7.4. Institutional Review Board Statement

Not applicable.

7.5. Informed Consent Statement

Not applicable.

7.6. Declaration of Competing Interest

The authors declare that they have no known competing financial interests or personal relationships that could have appeared to influence the work reported in this paper.

8. References

[1] Hong, P., Quan, W., Chen, Z., Liu, X., & Gao, S. (2025). Visual Anomaly Detection through the Joint Entropy-Energy Optimization for High-Speed Railway Traction Substation. IEEE Transactions on Instrumentation and Measurement, 74. doi:10.1109/TIM.2025.3554319.

[2] Fan, S., Liu, J., Li, L., & Li, S. (2024). Noise Separation Technique for Enhancing Substation Noise Assessment Using the Phase Conjugation Method. Applied Sciences (Switzerland), 14(5), 1761. doi:10.3390/app14051761.

[3] Priyadarsini, M., & Sonekar, N. (2025). A CNN-based approach for anomaly detection in smart grid systems. Electric Power Systems Research, 238, 111077. doi:10.1016/j.epsr.2024.111077.

[4] Chen, W., Liu, Y., Gao, Y., Hu, J., Liao, Z., & Zhao, J. (2024). Intelligent Substation Noise Monitoring System: Design, Implementation and Evaluation. Energies, 17(13), 3083. doi:10.3390/en17133083.

[5] Srivastava, A. K., Pandey, S., Ahmed, A., Basumalik, S., & Sadanandan, S. K. (2025). Synchrophasor Data Anomaly Detection for Wide-Area Monitoring and Control in Cyber-Power Systems. Smart Cyber-Physical Power Systems: Fundamental Concepts, Challenges, and Solutions, 1, 425–449. doi:10.1002/9781394191529.ch17.

[6] Melo, J. V. J., Lira, G. R. S., Costa, E. G., Vilar, P. B., Andrade, F. L. M., Marotti, A. C. F., Costa, A. I., Leite Neto, A. F., & Santos Júnior, A. C. dos. (2024). Separation and Classification of Partial Discharge Sources in Substations. Energies, 17(15), 3804. doi:10.3390/en17153804.

[7] Amusan, O., & Wu, D. (2025). Anomaly Detection and Localization via Graph Learning. Energies, 18(6), 1475. doi:10.3390/en18061475.

[8] Xu, L., Qiu, N., Yang, B., & Peng, S. (2023). Separation of Urban Substation Noise and Environmental Noise based on Independent Component Analysis. Journal of Physics: Conference Series, 2427(1), 012021. doi:10.1088/1742-6596/2427/1/012021.

[9] Itai, U., Bar Ilan, A., & Lazebnik, T. (2026). Tighten the lasso: a convex hull volume-based anomaly detection method. International Journal of Data Science and Analytics, 21(1), 32. doi:10.1007/s41060-025-00928-3.

[10] Zhou, T., Wang, Y., Lin, Y., Ai, B., & Liu, L. (2024). Deep Learning and Hybrid Fusion-Based LOS/NLOS Identification in Substation Scenarios for Power Internet of Things. IEEE Internet of Things Journal, 11(20), 33903–33914. doi:10.1109/JIOT.2024.3432798.

[11] Fan, S., Li, J., Li, L., & Chu, Z. (2022). Noise Annoyance Prediction of Urban Substation Based on Transfer Learning and Convolutional Neural Network. Energies, 15(3), 749. doi:10.3390/en15030749.

[12] Shao, X., Jiang, Y., Jiang, H., & Li, J. (2024). Research on substation intrusion event identification method based on MTF and CNN. Measurement Science and Technology, 35(2), 26104. doi:10.1088/1361-6501/ad092f.

[13] Yang, F., & Li, X. (2023). Research on Substation Monitoring and Fault Diagnosis Based on Distributed Computing and Artificial Neural Network. Parallel Processing Letters, 33(3), 2340004. doi:10.1142/S0129626423400042.

[14] Yan, C., & Razmjooy, N. (2023). Kidney stone detection using an optimized Deep Believe network by fractional coronavirus herd immunity optimizer. Biomedical Signal Processing and Control, 86, 104951. doi:10.1016/j.bspc.2023.104951.

[15] Liu, Z., Wang, Y., Wang, Q., & Hu, M. (2025). Vision Transformer-Based Anomaly Detection in Smart Grid Phasor Measurement Units Using Deep Learning Models. IEEE Access, 13, 44565–44576. doi:10.1109/ACCESS.2025.3549679.

[16] Kale, A. P., Wahul, R. M., Patange, A. D., Soman, R., & Ostachowicz, W. (2023). Development of Deep Belief Network for Tool Faults Recognition. Sensors, 23(4), 1872. doi:10.3390/s23041872.

[17] Alqahtani, N., Alam, S., Aqeel, I., Shuaib, M., Mohsen Khormi, I., Khan, S. B., & Malibari, A. A. (2023). Deep Belief Networks (DBN) with IoT-Based Alzheimer's Disease Detection and Classification. Applied Sciences (Switzerland), 13(13), 7833. doi:10.3390/app13137833.

[18] Abualigah, L., Elaziz, M. A., Sumari, P., Geem, Z. W., & Gandomi, A. H. (2022). Reptile Search Algorithm (RSA): A nature-inspired meta-heuristic optimizer. Expert Systems with Applications, 191, 116158. doi:10.1016/j.eswa.2021.116158.

[19] Houssein, E. H., Saad, M. R., Hashim, F. A., Shaban, H., & Hassaballah, M. (2020). Lévy flight distribution: A new metaheuristic algorithm for solving engineering optimization problems. Engineering Applications of Artificial Intelligence, 94, 103731. doi:10.1016/j.engappai.2020.103731.

[20] Samareh Moosavi, S. H., & Bardsiri, V. K. (2019). Poor and rich optimization algorithm: A new human-based and multi populations algorithm. Engineering Applications of Artificial Intelligence, 86, 165–181. doi:10.1016/j.engappai.2019.08.025.

[21] Dehghani, M., & Trojovský, P. (2021). Teamwork optimization algorithm: A new optimization approach for function minimization/maximization. Sensors, 21(13), 4567. doi:10.3390/s21134567.

[22] Zhao, W., Zhang, Z., & Wang, L. (2020). Manta ray foraging optimization: An effective bio-inspired optimizer for engineering applications. Engineering Applications of Artificial Intelligence, 87, 103300. doi:10.1016/j.engappai.2019.103300.